

Preparation and Properties of Mesoporous Carbon Composite as Negative Electrode Materials

Zhengping Zhao^{1,2}, Sitao Shen², Feng Chen², Mingqiang Zhong² and Jia Wei Chew^{3,*}

¹ Zhijiang College, Zhejiang University of Technology, Hangzhou 310014, China

² College of Materials Science and Engineering, Zhejiang University of Technology, Hangzhou 310014, China

³ School of Chemical and Biomedical Engineering, Nanyang Technological University, 637459, Singapore

*E-mail: xxsimen@163.com

Received: 5 June 2019 / Accepted: 6 August 2019 / Published: 7 October 2019

Using sodium lignosulfonate as carbon source, microspheres were prepared by ultrasound. Molybdenum disulfide was synthesized directly by hydrothermal method and grown on the surface of lignin microspheres. Then, molybdenum disulfide modified porous microsphere carbon material was prepared by pyrolysis at high temperature and used as the cathode material of lithium ion battery to study its electrochemical properties. The size of lignin microspheres was about 500 nm. The spacing of the molybdenum disulfide coating on the surface was 0.52 nm. After sintering, the diameter of microspheres is about 300 nm and the surface aperture of MoS₂@C microspheres is about 300 nm. The initial charge-discharge specific capacity was 1049 mAh/g, and the retention rate of 200 charge-discharge specific capacity was 87.3%. The scanning rate of cyclic voltammetric curves show that the electrical properties of MoS₂@C microspheres are stability.

Keywords: Lignin, MoS₂@C microspheres, Hydrothermal method, Electrochemical properties

1. INTRODUCTION

Lithium ion batteries have carbon as the negative electrode and lithium ion insertion compounds as the positive electrode [1-3]. The delinking and embedding process of lithium ion is the charging and discharging process of lithium ion battery. During the process of delinking and embedding, the electron delinking and embedding are also accompanied by the same amount of lithium ion. And the lithium ions are inserted/released and embedded/released back and forth between the negative and positive poles [4].

Nowadays, most of the cathode materials for lithium ion batteries are carbon materials, such as carbon fiber, natural graphite and artificial modified graphite. In recent years, the research on the cathode

materials of lithium ion batteries are mainly focuses on the surface modification of carbon materials, the adhesion of nano phases on the surface of the cathode materials, the formation of nano pores on surface, and other applications of nanotechnology [5-6]. Many achievements have been made in this field, which shows that lithium ion batteries have a promising future.

Lignin is an amorphous polymer with molecular structure containing oxyphenylpropanol or its derivatives, which formed by four alcohol monomers (p-coumarol, conitol, 5-hydroxyconitol, and erucyl alcohol). Lignin contains a variety of active functional groups, such as hydroxyl, carbonyl, carboxyl, methyl and side chain structure [7-10]. Among them, hydroxyl group was found more in lignin, like the form of alcohol hydroxyl groups and phenol hydroxyl groups. The amount of phenolic hydroxyl group directly affects the physical and chemical properties of lignin. For example, it can reflect the degree of etherification and condensation of lignin, as well as measure the solubility and reaction capacity of lignin. On the side chain of lignin, there are ester-type structures such as hydroxybenzoic acid, vanilla acid, syringic acid, hydroxycinnamic acid, ferulic acid, etc [11]. These ester-type structures exist in the side chain. In addition to ester-type structure, it is also ether-type connection or carbon-carbon connection as a biphenyl structure in the side chain site. Like phenolic hydroxyl, the side chain structure of lignin is directly related to its chemical reactivity.

Molybdenum disulfide composite carbon material, which is a modification of the gauge mesoporous carbon material. The material is in the regulation of mesoporous carbon microspheres grow many layers of flaky molybdenum disulfide, with a high specific surface area, good electrochemical performance, good dimensional stability and larger pore volume, then can be widely used in anode materials for lithium ion batteries.

Using sodium lignosulfonate as carbon source. The polyphosphazene microspheres were synthesized by appropriate solvent and ultrasonic. MoS_2 was grown on the lignin surface by direct hydrothermal. After then, MoS_2 modified porous carbon microspheres materials were obtained through the pyrolysis. Finally, the electrochemical properties of the samples were tested and analyzed to develop a kind of high performance lithium ion battery cathode material which can utilize lignin as carbon source.

2. EXPERIMENTAL SECTION

2.1 Materials

Sodium lignosulfonate, isopropyl alcohol, sodium molybdate, thiourea, potassium hydroxide, acetylene black, N-methylpyrrolidone and polyvinylidene fluoride (PVDF) were all analytical reagents purchased from Shanghai Chemical Reagents Corp (Shanghai, China).

2.2 Preparation of MoS_2 @C microspheres

Sodium lignosulfonate was weighed at 0.5 g to prepare an aqueous solution with a concentration of 0.05 g/ml. Ultrasound for 10 min until complete dissolution. The configured 10 ml solution was extracted and injected into 40ml isopropyl alcohol at a speed of 20 ml/h with an automatic sampler and followed ultrasound at 150 w for 1h. 0.151 g thiourea and 0.237 g sodium molybdate were weighed and

added to the high-pressure reactor together with the droplet suspension. After the reaction for a period of time, the high-pressure reactor was removed, and the product was cooled, centrifuged, washed and dried for 24 h. After the product is completely dried, put it into tube furnace for pyrolysis at high temperature. After pyrolysis, the MoS₂@C microspheres were prepared by grinding and sieving.

2.3 Battery assembly

Copper sheets with a radius of 1 cm were prepared by tablet pressing mechanism. Ethanol ultrasonic cleaning, blow-drying and weighing of each copper sheet were conducted. Acetylene black is grinding sieving reserve. PVDF and NMP were configured as conductive gels at a mass ratio of 1:10. Dissolved under 55 °C, and stirring until the gel without air bubbles once every 15 min. The MoS₂@C microspheres, acetylene black and conductive gel were added to the sample bottle at a ratio of 8:1:1. An appropriate amount of NMP was added, stirred for 30min and the sample was coated on the copper sheet. Dry electrodes with pressing machine, then vacuum drying at 60 °C by for 24 hours to prepare electrode materials and assembled into CR 2025 button cell [12, 13].

2.4 Characterization

FT-IR spectra of all samples were recorded using polymer granule on a Perkin-Elmer Wellesley MA spectrophotometer. Thermogravimetric analysis (TGA) was performed on a TGA 7 instrument (PerkinElmer) thermal analysis system. Sample weight taken was 2-4 mg. All the experiment data were taken as an average of at least five measurements. The microstructures were observed on a Scanning Electron Microscope (Hitachi S4000, Japanese) and a Transmission Electron Microscope (JEM-100CX II, Japanese). Raman spectroscopy is a method for qualitative analysis of molecular structure. The chemical structures were observed on a Lab RAM HR UV800 laser Raman spectrometer (JOBIN YVON, France). The excitation light source is 632.81 nm and the scanning range is 200~4000. The XPS (KRATOS AXIS Ultra DLD, Shimazu KRATOS) was used. The light source was Al-KαX rays and the vacuum degree was 3*10⁻⁷ Pa. Nitrogen adsorption test (BET) was using the automatic physical adsorption instrument (ASAP2020, mack instruments). X-ray diffractometer (X'pert PRO, PANalytical) was used. The test parameters of the instrument are as follows: 36 kV, 30 mA and Cu radiation.

The constant charge-discharge performance was tested after the sample electrode material was assembled into CR 2025 button battery. The electrochemical performances such as power density, energy density and specific capacitance can be obtained by processing and analyzing the results of constant current charge-discharge test [14]. The calculation formula of specific capacitance is:

$$C_s = I\Delta t/m\Delta V \quad (1-1)$$

Where I(A) is the charge-discharge current. Δt for discharge time. m is the mass of the active substance in the electrode material. ΔV is the discharge voltage range.

The cyclic voltammetry is to discuss the reaction of capacitor electrode after applying triangular waveform potential. The applied control signal is potential, and the measured corresponding signal is

current. It is mainly to study the change rules of I-t and I-U. The relation curve of U-I can be obtained by observing the T-t graph [15].

3. RESULTS AND DISCUSSION

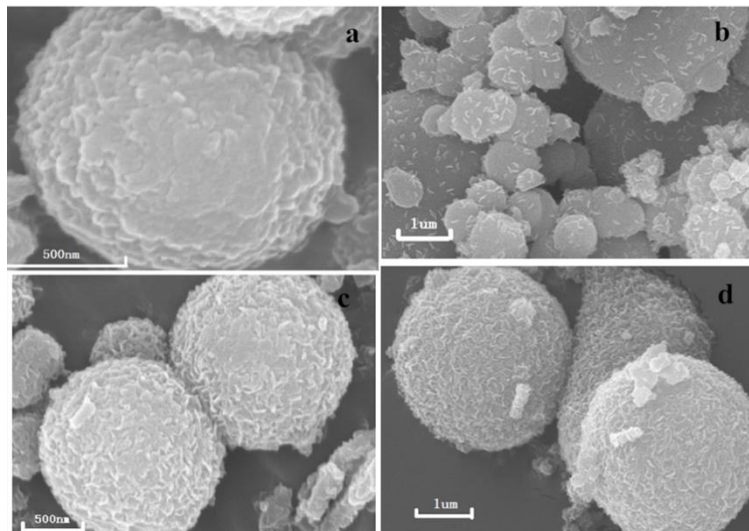


Figure 1. SEM of MoS₂@C microspheres.

Figure 1 is the scanning electron micrograph of the MoS₂@C microspheres. As can be seen from the figure, the sample has a regular microspherical structure. Molybdenum disulfide was mounted on the surface of the microsphere. It has a large specific surface area, which provides good conditions for lithium ion insertion and release. Combined with BET results, the microsphere is of multi-pore structure, providing a channel for the transmission of lithium ions.

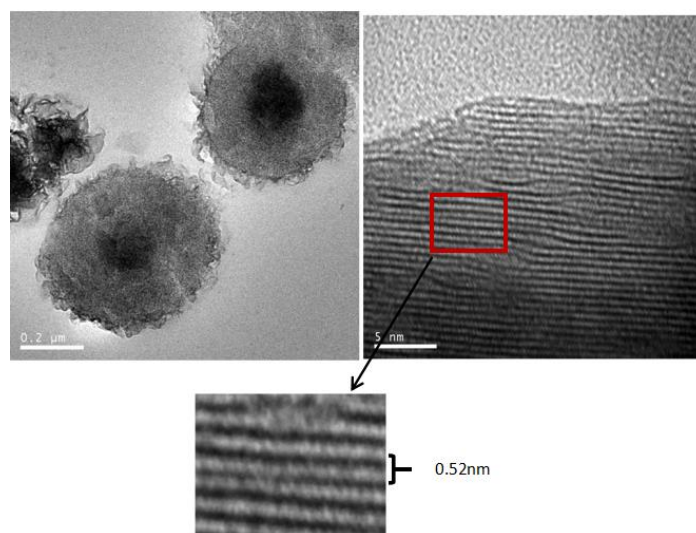


Figure 2. TEM of MoS₂@C microspheres.

Figure 2 shows the transmission electron micrograph of the sample. As seen in figure, the sample is spherical. The microsphere is similar to a core-shell structure, with a black center and a light-colored substance. The center of the microsphere is the carbon skeleton after lignin pyrolysis, namely the microporous carbon sphere. Wrapped in the carbon sphere is hydrothermal synthesis of molybdenum disulfide, a lamellar structure, and layer spacing of 0.52 nm. The formation of lamellar carbon materials is due to the precipitation polymerization of polyphosphonitrile [16]. During the sintering process, small molecules spill out and form skeletons into carbon. Lamellar structures provide channels for the emergence and insertion of lithium ions. Like molybdenum disulfide, it is also lamellar and allowing lithium ions to escape and embed.

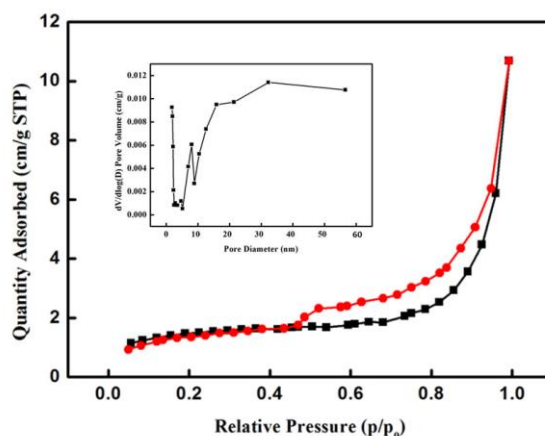


Figure 3. Nitrogen adsorption-desorption curves of porous carbon spheres and the distribution of pore sizes

Table 1. The specific surface area, pore volume, pore diameter of MoS₂@C microspheres

specific surface area (m ² /g)	pore volume (cm ³ /g)	pore diameter (nm)
4.93	0.016	147.5
3.60	0.009	162.9
3.54	0.012	115.4
4.52	0.019	225.3

Nitrogen adsorption curves is a typical IV model samples. Under strong low pressure, the BET curve shows a gentle trend. As the pressure increases, the curve starts to go up, explosively. It indicates that there are a large number of microporous structures in the sample, and the high pressure growth of BET curve is mainly caused by mesoporous effect. A large amount of condensation in the nanometer pore channel, leading to rapid growth. The adsorption curve shows that the surface pores of the microspheres are nano-scale, which verifies the abrupt change of high-pressure nitrogen adsorption. The

adsorption and desorption curves do not coincide, and the micropores are basically concentrated at the nanometer level. With the increase of hydrothermal synthesis time, molybdenum disulfide was synthesized by coating carbon source materials.

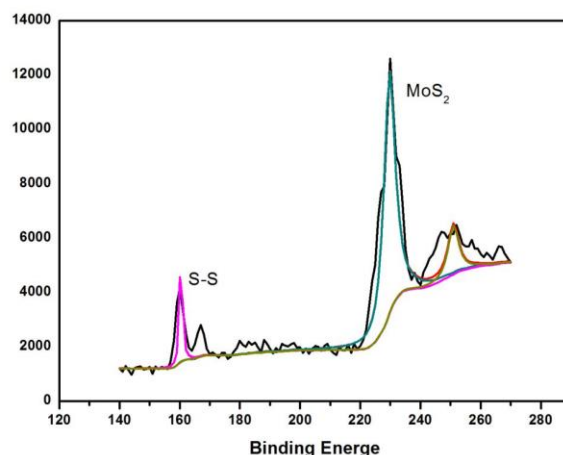


Figure 4. The XPS spectrum of S

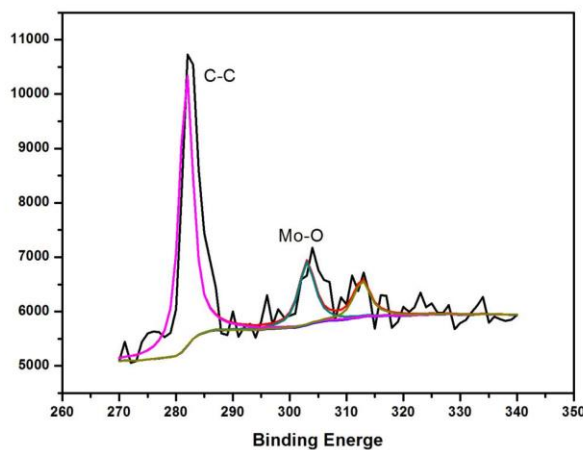


Figure 5. The XPS spectrum of C and Mo-O

The XPS spectra were analyzed as shown in figure 4, 5 and 6. The carbon in the sample mainly form C-C bond, which is consistent with the experimental design results [17]. The final product is the carbon skeleton after lignin pyrolysis. In the sample, S mainly exists in MoS₂, but there are also many SO₂ structures. The main reason may be that in the process of tube furnace pyrolysis, oxygen is not completely eliminated and molybdenum disulfide is oxidized. Most Mo existed in MoS₂, indicating that the hydrothermal synthesis reaction was successful and the experimental conclusion was verified. There are also many Mo-O bonds, which are consistent with the reason for the existence of SO₂ [18]. Oxidation of molybdenum disulfide occurs in the sample, which verifies the correctness of the experiment.

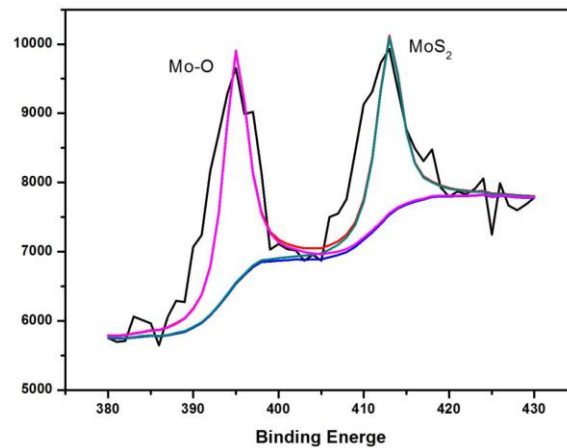


Figure 6. The XPS spectrum of Mo-O and MoS₂

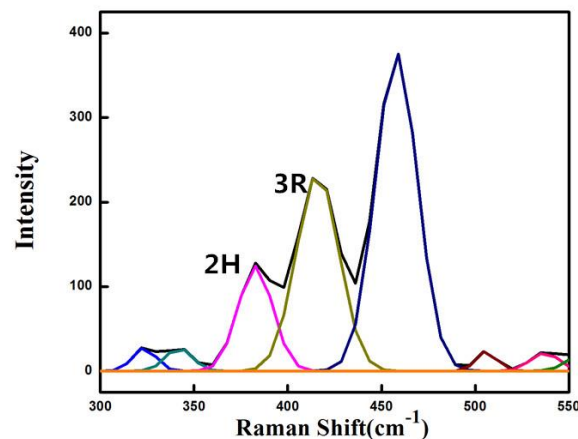


Figure 7. The Raman spectrogram of the sample

Figure 7 is the Raman spectrum of the sample, which contains two vibration modes of molybdenum disulfide, E12g and A1g. As can be seen from the figure, E12g is the in-plane vibration, while A1g is the out-of-plane vibration. The Raman spectra of 350-550 cm^{-1} are only partial spectra of molybdenum disulfide. The peak position of molybdenum disulfide in Raman spectrogram is related to the number of layers of molybdenum disulfide [19]. As the number of molybdenum disulfide layers increases, the van der Waals force decreases. The vibration mode of E12g has red shift, and the vibration mode of A1g is opposite to that of E12g. The peak of monolayer molybdenum disulfide E12g was near 385 cm^{-1} , while the peak of A1g was 403. As can be seen from the figure, the first two peaks belong to molybdenum disulfide peaks, which are 380 and 420 cm^{-1} , respectively [20]. It is verified that molybdenum disulfide exists in the form of multilayer stacking in the sample.

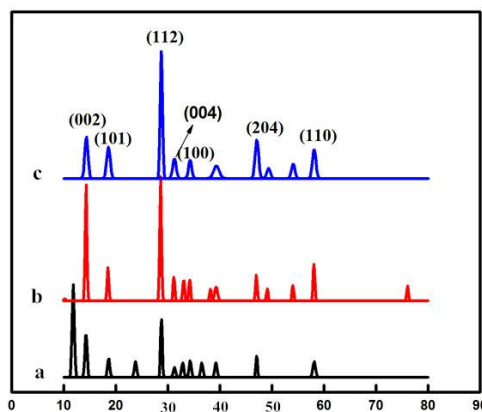
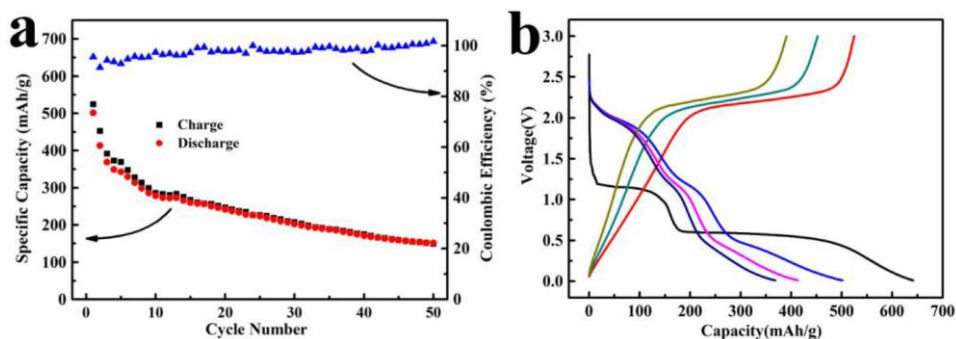


Figure 8. The XRD spectrum of samples

Figure 8 shows the XRD curve of the samples. The figure shows that $2\theta=14^\circ$ of (002) peak, $2\theta=29^\circ$ of (112) peak, and (110), (204), (110) are the existence of the characteristic peaks of MoS_2 [21-22]. The experiment of hydrothermal synthesis of molybdenum disulfide is relatively perfect single layer. Molybdenum disulfide monolayer or multilayer lamellar structure is conducive to the insertion and release of lithium ions. The lamellar structure increases the specific surface area of the material and further improves the electrochemical properties of carbon materials. The experimental results show that the hydrothermal synthesis of molybdenum disulfide best temperature is 200°C . $\text{MoS}_2@\text{C}$ microspheres surface contain oxygen functional group structure, which needs to be pyrolyzed at high temperature. Molybdenum disulfide is a very easy to be oxidized at high temperature, and it is a lamellar structure on the surface of the material. Larger the surface area, more easily oxidized. Therefore, molybdenum disulfide was synthesized by high temperature hydrothermal method. The higher the water temperature, the more complete the package of composite carbon materials and easy to oxidation in the tube furnace.



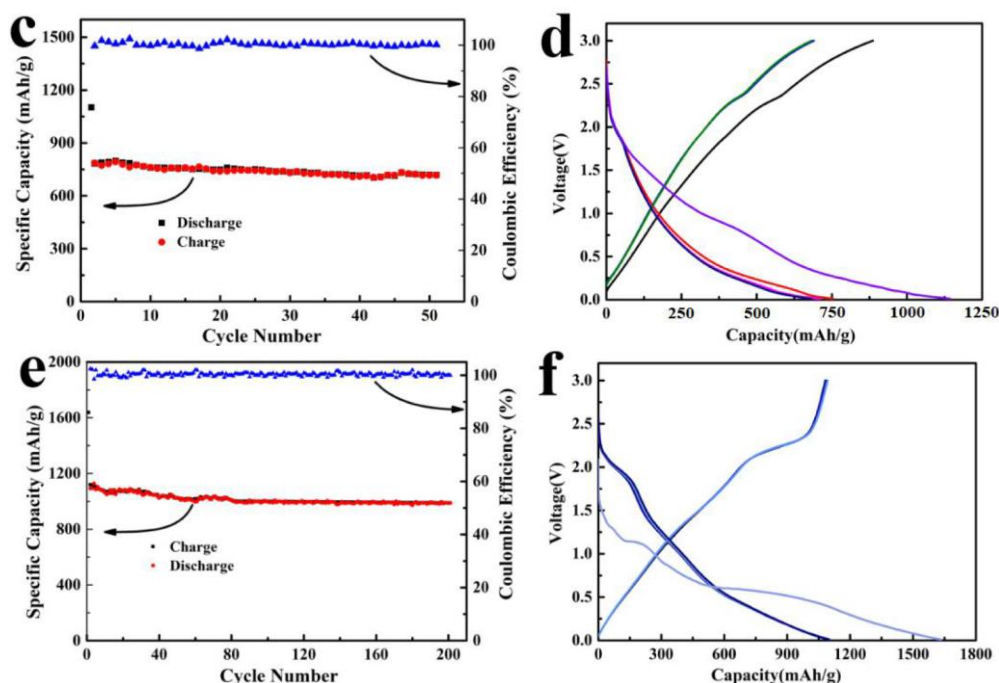


Figure 9. The charge-discharge data and cycling performance of C microspheres (a-b), MoS₂ (c-d), MoS₂@C microspheres (e-f).

Figure 12 is the cycling performance results of three kinds of pure C microspheres, MoS₂ and MoS₂@C microspheres under the current density of 0.1 A·g⁻¹. Figure 12b shows the first three charge and discharge curves of C microspheres. Figure 12c is the corresponding cyclic performance diagram, and it can be seen that the specific capacity of the agglomerated flower MoS₂ declines rapidly. The first discharge curves appear in two voltage platforms of 1.1 V and 0.5 V, corresponding to the process of Li⁺ embedding to form Li_xMoS₂ and Li_xMoS₂ conversion to form Mo and Li₂S. After the first discharge, the material becomes a mixture of Mo and Li₂S nanoparticles. In the following charging and discharging process, it actually turns into the conversion reaction between Li₂S and S, which is the typical charging and discharging mode of li-s batteries. Mo atoms generated by the first discharge have a high affinity for sulfur separators. The suspended bond on the surface can attract and fix polysulfone, and can be used as the adsorption site for lithium ions in subsequent cycles to improve the electrochemical activity of the materials. Figure 12d shows the first three charge and discharge curves of C microspheres. In the first discharge, a platform appears around 1.0 V, which is due to the relatively large specific surface area of the material. During the embedding of Li⁺ into the electrode material, SEI film is generated on the surface and consumes more Li⁺, so the platform is long and the voltage is low. In the next few discharges, no more SEI branes are generated, so there is no platform in the curve. At the same time, weak platforms can be found in the three charging curves, indicating that in the process of removing Li⁺, in addition to Li⁺ in the middle of carbon layer, a lot of Li⁺ comes from nanopores in the material. Figure 12c shows the specific capacity of the first 50 cycles. It is not difficult to find that the presence of s-doped elements increases the lattice defect of carbon material and the active site of reaction, which makes its specific capacity much higher than that of commercial graphite negative electrode. Meanwhile, its cyclic stability is also very good, stable at 728 mAh·g⁻¹.

Compared to C microspheres, MoS₂ and MoS₂@C microspheres performance has improved greatly, and can be found from figure 12f, combined with the characteristics of the two materials composite microspheres, discharge curve has three platform, for the first time around 1.0 V combines MoS₂ and MoS₂@C microspheres both mechanism of Li⁺ platform is more obvious, but due to the low material specific surface area, therefore platform is narrow. Secondly, of all the discharge curve, can not only see about 2.2 V peak, also can see weak around 1.2 V curve slope change, the presence of nanopores in that microspheres, but because of molybdenum disulfide tightly coated carbon ball surface, in the process of a few times before, electrolyte can't arrive every part of the materials, lead to three times before the charge and discharge efficiency is low, lower than capacitance quickly. Figure 12e clearly see material with high specific capacity at the same time, the carbon cycle stability without the ball in the late of good, because the MoS₂@C microspheres outer molybdenum disulfide is mostly composed of flake MoS₂, in the long process of charging and discharging will inevitably appear in pulverization after burst out of microsphere surface caused by specific capacity decline. Surprisingly, after 200 cycles there was a capacity of 1049 mAh·g⁻¹, which equalled a capacity retention rate of 93%.

The comparison of MoS₂@C microspheres and other anode materials were added in table 2.

Table 2. The capacity of anode materials

anode materials	capacity (mAh·g ⁻¹ , 100 cycles)	retention rate (%, 100 cycles)
petroleum carbon [2]	264	77.0
MoS ₂ @C microspheres	1167	93.2
NiO@carbon [5]	573	84.4
S@Li@carbon [16]	1294	87.8
Si@carbon [18]	3241	71.2

As can be seen from table 2, traditional petroleum carbon anode materials have a lower specific capacity and the corresponding 100 cycle retention rate is also low. It is also verified that only the embedding and stripping of lithium ions exist in the charging and discharging process of petroleum carbon anode materials. The specific capacity of the battery is also proportional to the graphitization degree of the carbon material. The higher the graphitization degree, the higher the specific capacity. However, its maximum specific capacity is 372 mAh·g⁻¹, which is much lower than the application of transition metal or metal oxide as anode material. Si has the highest specific capacity, which is 3241 mAh·g⁻¹ after 100 charge and discharge cycles, but has the defect of large expansion coefficient. While the higher cycles, the reduction in specific capacity is more significant. It is mainly caused by the crushing of Si grains. S@Li is one of the research hotspots of lithium ion battery anode materials, but its specific capacity retention rate is still lower than MoS₂ after 100 cycles. Limited by the specific capacity of MoS₂ material itself, the materials listed in the table are in the middle. However, MoS₂@C microspheres have the highest specific capacity retention rate. And the specific capacity is 5 times that of petroleum carbon, which has a high application value. Due to the influence of their conductivity or volume expansion, other transition metals or metal compounds need to be prepared with carbon materials

as negative materials. However, these anode materials are all in the experimental research stage, but fewer are widely used. Therefore, there is still a long way before the real large-scale application, which requires new breakthroughs in structural design and manufacturing.

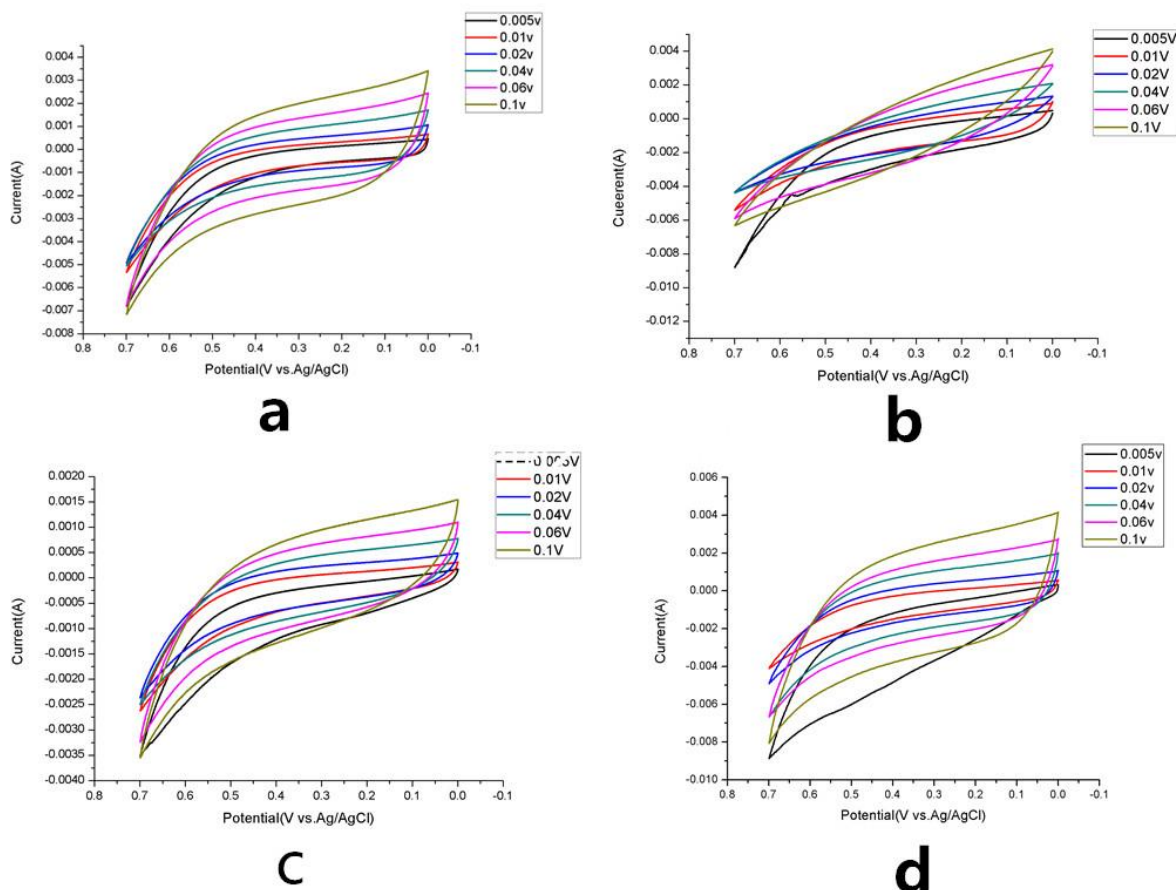


Figure 10. The cyclic voltammograms of the sample

Figure 10 is the cyclic voltammograms in 0.005 V/s, 0.01 V/s, 0.02 V/s, 0.04 V/s, 0.06 V/s, 0.1 V/s scanning rate, respectively. It can be seen from the figure, the electrochemical properties are stable and the electric quantity is large.

4. CONCLUSIONS

Sodium lignosulfonate was used as the only carbon source, modified in a reasonable way and then layered molybdenum disulfide was grown on by hydrothermal method. After carbonization, the lignin microspheres still have regular spherical structure and good dispersion. Molybdenum disulfide is uniformly distributed on the surface of carbon spheres in regular lamellar shape. Lamellar molybdenum disulfide significantly improved the electrochemical properties of the sample, but with the thickening of the lamellar structure. The stability of the material decreased significantly. Molybdenum disulfide hydrothermal synthesis and coated the best temperature is 200 °C. The amount of molybdenum disulfide

increased with the reaction time. The results of constant current charging and discharging show that the unit capacitance is 1049 mAh/g higher than 372 mAh/g of pure carbon material when the current density of porous carbon material is 1.0 A/g after 200 times of charging and discharging. Lignin carbon material can be used as the cathode material of commercial battery.

ACKNOWLEDGEMENTS

We are thankful for the Technology Project of Keqiao Innovation Research Institute of Zhejiang University of Technology (2018KQ002), Project Supported by Zhejiang Provincial Natural Science Foundation of China (LY18E030009, LQ14E030004, LQ18E030013) and National Natural Science Foundation of China (21504079) for the support to this research.

References

1. I. H. Kim and K. B. Kim. *J. Electrochem. Soc.*, 153 (2006) 383.
2. A. Oya and N. Kasahara. *Carbon*, 38 (2000) 1141.
3. W. W. Luken and G. D. Stucky. *Chem. Mater.*, 14 (2002) 1665.
4. Z. Li and M. *Chem. Mater.*, 15 (2003) 1327.
5. J. Jang and B. Lim. *Adv. Mater.*, 14 (2002) 1390.
6. J. Jang, B. Lim and M. Choi. *Chem. Comm.*, 33 (2005) 4214.
7. J. E. Hampsey, Q. Y. Hu and L. Rice. *Chem Comm.*, 28 (2005) 3606.
8. S. H. Joo, S. J. Choi and I. Oh. *Nature*, 412 (2001) 169.
9. M. Kruk, M. Jaroniec, T. W. Kim. *Chem. Mater.*, 15 (2003) 2815.
10. A. H. Lu, W. Schmidt and B. Spliethoff. *Adv. Mater.*, 15 (2003) 1602.
11. Y. Xia and R. Mokaya. *Adv. Mater.*, 16 (2004) 1553.
12. A. K. *Solid State Ionics*, 69 (1994) 212.
13. A. B. Fuertes and S. *Carbon*, 42 (2004) 3409.
14. A. B. Fuertes and T. A. *J. Mater. Chem.*, 15 (2005) 1079.
15. Z. P. Zhou, Z. P. Zhao and M. Q. Zhong. *Electrochim. Acta*, 274 (2018) 288.
16. Y. Qian, Y. Deng and X. Qiu. *Green Chem.*, 16 (2014) 2156.
17. F. Chen, W. J. Zhou, H. F. Yao, P. Fan, J. T. Yang, Z. D. Fei and M. Q. Zhong. *Green Chem.*, 15 (2013) 3057.
18. R. Ryoo, S. H. Joo and S. Jun. *J. Phys. Chem. B.*, 103 (1990) 7743.
19. E. W. Zhang and H. L. Zhang, *Int. J. Electrochem. Sci.*, 13 (2018) 12380.
20. G. R. Li, Z. P. Feng and Y. N. Ou. *Langmuir*, 26 (2010) 2209.
21. B. P. Bastakoti, H. Oveisi and C. C. Hu. *Eur. J. Inorg. Chem.*, 7 (2013) 1109.
22. M. Oschatz, S. Thieme and L. Borchardt. *Chem. Commun.*, 49 (2013) 5832.